Green Chemistry

PAPER

View Article Online
View Journal

Cite this: DOI: 10.1039/d4gc06546h

Assessing supported nickel catalysts for the upcycling of real WEEE plastics through low-pressure hydropyrolysis and dehalogenation†

Lidia Amodio, [a,b] Jennifer Cueto, [a] Julio López,[a,b] Héctor Hernando,[a] Patricia Pizarro [a,b] and David P. Serrano *[a,b]

Electrical and electronic equipment waste (WEEE) is among the fastest-growing waste streams, posing recycling challenges due to its high heterogeneity and the presence of organo-halogenated compounds. Hydropyrolysis offers a promising way to convert WEEE plastics into valuable, dehalogenated organic liquids, facilitating their upcycling. This study examines catalytic hydropyrolysis at mild pressure of real WEEE plastics containing both chlorine and bromine. Nickel-based catalysts on various supports (Al_2O_3, n-ZSM-5 zeolite, SiO_2, and activated carbon (AC)) were tested in batch and continuous systems. In the thermal reaction, over 70 wt% oil was obtained, decreasing slightly with catalyst use. Char played a key role in removing halogens, retaining up to 95%, which was reinforced by the dehalogenation activity of the catalysts. While all catalysts were highly efficient for oil dehalogenation, the best performance was shown by Ni/AC. The AC support alone contributed significantly to halogen trapping, while Ni incorporation into the catalyst further enhanced the oil dehalogenation degree, allowing total Br removal and reducing its Cl content to just 9 ppm, as well as enhancing the production of valuable monoaromatic hydrocarbons. The Ni/AC catalyst exhibited high stability over time on stream when using a continuous oil feeding reaction system and could be fully regenerated by water/dioxane washing, restoring its dehalogenation capability to the level of the fresh one. This work highlights the potential of catalytic hydropyrolysis to address the environmental challenges posed by WEEE plastics, offering a sustainable alternative for their dehalogenation and upcycling into valuable chemical products.

Received 27th December 2024,
Accepted 6th March 2025

DOI: 10.1039/d4gc06546h

rsc.li/greenchem

Green foundation

1. This work proposes a catalytic hydropyrolysis process to upcycle real WEEE plastics into valuable dehalogenated oils, in agreement with the principles of reducing hazardous substances, promoting sustainable resource recovery and decreasing environmental risks. It proceeds using heterogeneous catalysts under vapor phase conditions, with the former then being easily recovered and reused.

2. Using a Ni/activated carbon catalyst, a highly effective dehalogenation of both Cl- and Br-containing species is achieved, yielding aromatic hydrocarbon-rich oils suitable as raw chemical sources. Accumulation of halogens in the char fraction ensures their safe disposal. The process demonstrated scalability, with robust catalyst stability, offering a practical and eco-friendly solution for recovering valuable products from WEEE plastics.

3. To enhance its sustainability, future research could focus on the design of catalysts from bio-based or waste-derived carbon materials, further aligning the process with green chemistry principles.

1. Introduction

Plastics have become essential in our daily lives, offering significant advantages over traditional materials like metals and glass. Their versatility has led to the creation of hundreds of plastic variations, crucial for a wide range of industrial sectors, such as packaging, automotive, food, construction, agriculture and electrical/electronic.[1,2]

Plastic production has increased dramatically, rising from two million tonnes in 1950 to over 400 Mt annually in 2022.[3] The persistent nature of these materials and the challenges

[a]Thermochemical Processes Unit, IMDEA Energy Institute, Avda. Ramón de la Sagra, 3, 28935, Móstoles, Madrid, Spain. E-mail: david.serrano@imdea.org; Tel: +34 917371138
[b]Chemical and Environmental Engineering Group, Rey Juan Carlos University, c/Tulipán, s/n, 28933, Móstoles, Madrid, Spain

† Electronic supplementary information (ESI) available. See DOI: https://doi.org/10.1039/d4gc06546h

associated with their disposal have raised serious environmental concerns,[4] as plastic waste generation (around 350 Mt (ref. 5)) is now nearly equal to the production rate. Despite plastics being recognized for their potential mechanical recyclability, global production of recycled plastic reached only 35.5 million tonnes in 2022.[3] Several factors contribute to the low recycling rates of plastics, primarily stemming from poor waste management. Furthermore, factors such as contamination levels, the use of additives, and the gradual degradation of polymers over their lifecycle hinder effective plastic recycling.[6] Thus, mechanical recycling is the most effective strategy for separately collected, low-additive and well-preserved plastics, but its application to mixed or degraded plastic waste faces many challenges.[7]

Plastics found in Waste from Electrical and Electronic Equipment (WEEE) are particularly problematic due to their high heterogeneity in terms of polymers and additives, making them difficult to be separated using automated methods.[8] Common components in these plastics include chlorinated and brominated compounds. Thus, approximately 30% of these plastics contain halogenated flame retardants due to their effectiveness and compatibility with various types of plastics.[9] Chlorine can also be part of the polymeric chain, as in the case of PVC used for electric wiring in WEEE.[10] The presence of halogenated species complicates energy recovery through incineration due to their negative impacts on the environment and human health,[11,12] such as the formation of dioxins, PCBs and other extremely harmful species.[13] Landfilling is not recommended for PVC disposal since, in addition to involving a loss of resources, the relatively low energy of the C–Cl bond makes it prone to degradation under environmental conditions, such as sunlight and high temperatures, leading to the release of pollutants.[13] In contrast, chemical recycling techniques represent a promising route that can significantly improve recycling rates by effectively processing mixed plastic waste.[6,14] Among the various technologies being explored, pyrolysis stands out as an effective method for converting plastic waste into high-grade fuels or valuable chemicals due to its simplicity and versatility.[15,16] However, the presence of halogens in pyrolytic oils complicates their use as feedstock in refineries and petrochemical plants. While no universal legal limits exist, a common reference range for halogen concentration in oils is 10 to 50 ppm, though specific guidelines for bromine remain undefined.[17–19]

Among the existing techniques for decomposing halogen-containing organic compounds, hydrodehalogenation (HDH) involves the hydrogenolysis of carbon–halogen bonds and requires an external hydrogen supply and a supported metal catalyst.[20,21] The dehalogenation process can be performed either simultaneously with or sequentially after the decomposition of WEEE plastics.[21] Thus, an interesting option is the coupling of pyrolysis and halogen elimination through simultaneous hydropyrolysis and HDH. The initial use of hydrogen in pyrolysis for coal processing, and later for other raw materials, has proven crucial for hydrocarbon production.[22] In this way, hydrogen incorporation in biomass pyrolysis has demonstrated several advantages, like the formation of radicals that prevent catalyst coking caused by the polymerization of reactive volatile intermediates.[22,23] Additionally, the exothermic nature of hydrogen addition generates heat, supporting the sustainability of the endothermic pyrolysis reaction.[24]

In a previous study, using a commercial catalyst (Pd/Al_2O_3), we demonstrated the feasibility of applying hydropyrolysis to effectively convert highly halogenated real WEEE plastics into valuable products.[25] Building on these findings, the current work focuses on investigating various catalysts to further enhance the efficiency and selectivity of this innovative route. To that end, four distinct supports (silica,[26] activated carbon,[27] alumina,[28] and ZSM-5 zeolite[29]) have been selected, showing a wide range of properties. Based on the literature, these types of supports can be considered very promising for HDH,[20] although they have been scarcely tested with complex real residues like WEEE plastics. On the other hand, the most common metal active phases for HDH are noble metals such as Pd and Pt. However, given the typically high contaminant levels in WEEE and the complex reactions involved in hydropyrolysis, a more cost-effective metal, like Ni, could be a suitable alternative.[30] Hence, it has been incorporated here into the above-mentioned supports. The performance of these catalysts for the hydropyrolysis of WEEE plastics was initially evaluated in a batch reaction system. Subsequently, the stability over time on stream of the two best-performing catalysts was investigated in the hydroconversion/hydrodehalogenation of a thermal pyrolysis oil from WEEE plastics using a continuous flow reactor. Finally, the regenerability of the best performing catalyst (Ni/AC) was probed by solvent washing. This study highlights the importance of developing advanced recycling methods that align with circular economy principles, reducing the environmental impact of plastic wastes while promoting their valorization.

2. Materials and methods

2.1. Catalyst preparation and characterization

The Ni-based catalysts were prepared by wet impregnation of the Ni precursor ($NiNO_3{\cdot}9H_2O$, Alfa Aesar, purity: 99.9985%) onto four different supports: Al_2O_3 (Sigma Aldrich), n-ZSM-5 zeolite (Si/Al = 42, Clariant HCZP90), SiO_2 (Saint-Gobain NorPro), and activated carbon (AC, Honeywell). A theoretical Ni content of 2.5 wt% was loaded through a two-step wet impregnation method. In each step, half of the metal precursor was dissolved in Milli-Q water (10 ml of water per gram of support) and stirred in a rotary evaporator for 5 h at 60 °C and 200 rpm. After each impregnation, the solvent was removed using a rotavapor, followed by drying overnight at 60 °C for activated carbon[31] and 90 °C for the other catalysts. The non-carbonaceous catalysts were further calcined at 500 °C in a static air muffle furnace for 4 h, with a heating rate of 1.8 °C min^{-1}. Before the reactions, all catalysts were reduced in a tubular muffle furnace under a hydrogen flow of 100 ml min^{-1}. The reduction process was also carried out at 500 °C,

with this temperature being maintained for 2 h. All the prepared catalysts were characterized using different analytical techniques, as detailed below.

For the determination of the nickel content, the samples were treated with a 2 : 1 mixture of nitric and hydrofluoric acids, using an Anton Paar MW3000 microwave digestion system. The resulting solution was analyzed using inductively coupled plasma optical emission spectroscopy (ICP-OES) on a PerkinElmer Optima 7300 DV. X-ray diffraction (XRD) analyses were performed using a Philips PW 3040/00 X'Pert MPD/MRD diffractometer, with Cu-Kα radiation (wavelength λ = 1.5406 Å), operating at 45 kV and 40 mA. Diffraction patterns were collected over a 2θ range from 5 to 90°.

The textural properties of the catalysts were assessed through N_2 adsorption–desorption isotherms, recorded at 77 K using a Micromeritics TriStar II PLUS analyzer. Prior to the measurements, the samples were vacuum-degassed at 300 °C for 3 h. The surface area was calculated using the BET model, while the micropore volume and external surface area were determined using the *t*-plot method. The total pore volume was determined from the adsorption at P/P_0 = 0.98.

The acidity of the catalysts was evaluated by temperature-programmed desorption of ammonia (NH_3-TPD), using a Micromeritics AUTOCHEM 2910 instrument fitted with a thermal conductivity detector (TCD). For these measurements, 0.1 g of the sample was pre-treated by heating to 650 °C under a helium flow (50 ml min^{-1}) for 1 h to ensure degassing. The system was then cooled to 100 °C, and the adsorbate gas (10 vol% NH_3/He) was introduced for 30 minutes to facilitate adsorption. After removing the physisorbed gases with a helium purge, desorption profiles were recorded by increasing the temperature to 650 °C under a helium flow (50 ml min^{-1}). Field emission scanning electron microscopy (FE-SEM) was employed to investigate the morphology of the materials and assess the dispersion of Ni particles. The analysis was performed using a JEOL JSM-7900F scanning electron microscope with an energy-dispersive X-ray (EDX) analyser. Images of impregnated catalysts were acquired through transmission electron microscopy (TEM JEOL JEM 1400, 120 kV), whereas the particle size was determined using the SightX Viewer software, considering more than 150 particles for each catalyst.

2.2. Experimental setup and product characterization

2.2.1. Batch reaction system. The hydropyrolysis experiments were performed using as feedstock a real plastic waste from electrical and electronic equipment that was supplied by COOLREC (Netherlands). Table 1 summarizes the main properties of the raw plastic waste, whereas its detailed characterization can be found in our previous work.[25]

A scheme of the employed batch reaction system is presented in Fig. 1A. The detailed description and optimization of the system parameters were provided in a previous work, which was used here as a reference for selecting the operation conditions (temperatures of both thermal and catalytic zones, feedstock/catalyst ratio and gas flow rate). In summary, the reactor was equipped with two independently heated zones, with temperatures being monitored by K-type thermocouples. After loading 8 g of plastic waste into the thermal zone, the system was purged using a 50 vol% H_2/N_2 mixture. The upper catalytic zone, containing the Ni catalyst (3.2 g), was preheated to 350 °C and maintained under a N_2/H_2 flow rate of 100 ml min^{-1} for 30 minutes to ensure that Ni species were fully reduced before the reaction. After this period, the thermal zone was heated at a rate of 10 °C min^{-1} until reaching 550 °C and held at this temperature for 20 minutes.

During hydropyrolysis, a solid fraction (char) was formed in the thermal zone and remained there, while vapours passed through the catalytic bed. Non-condensable gases and condensable vapours (oil) moved through the catalytic zone, with the oil being collected in a stainless-steel condenser cooled in an ice bath. A back-pressure regulator (BPR) maintained the reactor pressure at 6 bar, and gas samples were taken with a continuous flow meter every 5 minutes using a gas sampling bag. The uncondensed gas stream was passed through a series of bubblers containing a sodium carbonate solution to capture halides.

2.2.2. Continuous liquid feeding reaction system. The pyrolysis oils used in this study were produced from WEEE plastics sourced from COOLREC through pyrolysis at atmospheric pressure, as detailed in our previous work.[32] Briefly, plastic waste particles were fed at a fixed rate of 5 g h^{-1} using a custom-built screw feeder (PID Eng&Tech, Spain) into a two-zone reactor under a nitrogen flow of 50 ml min^{-1}. The thermal zone was maintained at 575 °C to ensure complete pyrolysis of the plastic. For Feed-1, no catalyst was used in the catalytic zone, whereas Feed-2 was obtained using an Fe/n-ZSM-5 catalyst operating at 450 °C in the catalytic zone with a weight hourly space velocity (WHSV) of 2.5 h^{-1}. The composition of these two pyrolysis oils is given in Table 2.

Table 1 Characterization of raw WEEE plastics

Polymer composition[a] (%)					
ABS	(HI)PS	PP	PMMA	EVA	PC
75	33.3	33.3	16.7	16.7	8
Proximate analysis (wt%)					
Volatile matter		Fixed carbon		Ash	
89.1 ± 1.3		4.2 ± 1.2		6.7 ± 0.08	
Ultimate analysis (wt%)					
C		H	N	O	
77.2 ± 1.4		8.9 ± 1.6	4.6 ± 1.4	2.6 ± 1.5	
Halogen content (ppm)					
Cl				Br	
660 ± 40				890 ± 150	

[a] The percentage values represent the detection frequency of the polymers in the FT-IR analysis.

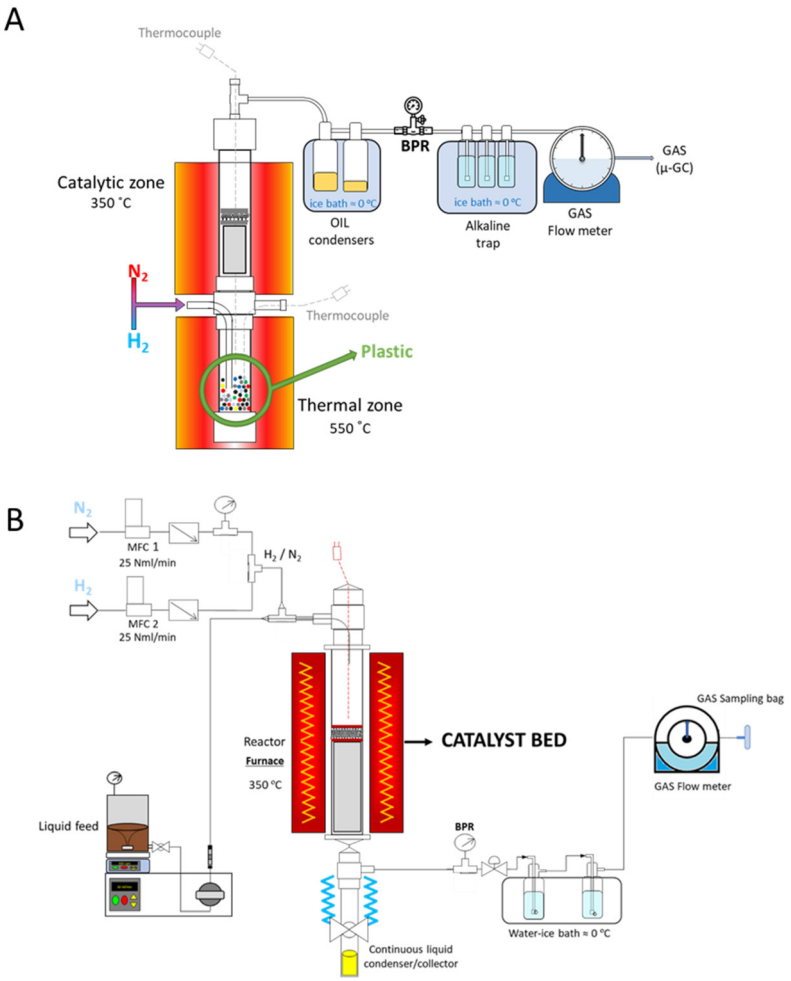

Fig. 1 (A) Batch and (B) continuous reaction systems used in the hydropyrolysis/hydrotreatment tests.

Table 2 Composition of pyrolysis oils

Molecular composition (wt%)						
Sample	M-AR	P-AR	ALIPH	O-Comp	N-Comp	$TOT_{Detected}$
Feed-1	43.4	1.6	11.3	11.8	9.7	77.8
Feed-2	55.2	0.4	14.2	5.8	2.7	78.3

Ultimate analysis (wt%)				
	C	H	N	O
Feed-1	83.4 ± 0.6	9.1 ± 1.3	3.4 ± 1.0	4.0 ± 1.6
Feed-2	85.2 ± 0.5	11.0 ± 0.4	1.2 ± 0.1	2.6 ± 1.0

Halogen content (ppm)		
	Cl	Br
Feed-1	273 ± 5	352 ± 3
Feed-2	80 ± 2	115 ± 2

To assess catalyst stability over time on stream, the pyrolysis oils were fed into a continuous-flow stainless-steel reactor (12 mm i.d., 250 mm length) (Fig. 1B). This setup enabled catalyst evaluation without interference from char formation, ensuring smooth operation in a continuous reaction system. The reaction conditions in the catalytic zone were those opti-

mized in the hydropyrolysis batch experiments, set at 350 °C and a pressure of 6 bar. A 50 vol% mixture of H_2 and N_2 was supplied *via* two independent mass flow controllers (MFCs), which were mixed before entering the reactor at a total flow rate of 50 ml min^{-1}. To ensure the reduction of the catalysts, the system was held at the reaction temperature for 30 minutes under a flow of H_2/N_2 (50 vol%). After this pre-conditioning treatment, an HPLC (Gilson HPLC pump 307) pump was activated to start feeding the oil stored in a pressurized vessel with magnetic stirring connected to the reactor. In order to provide a sufficient quantity of feedstock and to reduce its viscosity, the reactions were conducted by diluting the oil to 30% by weight in decalin (Thermo Scientific, 99%), which was used as a practical solution due to the limited amount of oil. The total feeding rate of pyrolysis oil + decalin was set at 10 mL min^{-1}. The catalyst loading in the fixed bed reactor was selected to operate with a weight hourly space velocity (WHSV) of 2.5 h^{-1}, referred to the pyrolysis oil feeding rate. At the reactor outlet, a stainless-steel condenser, provided with a ball valve, allowed the hourly measurement and analysis of the upgraded oil thus produced. The results, presented as hourly values, correspond to average operation times of 0.5, 1.5, 2.5, and 3.5 hours, respectively. A back-pressure regulator (BPR) maintained the desired pressure. Two bubblers filled with a 0.1 M Na_2CO_3 solution captured the halogenated compounds from the gas phase. Permanent gases and light hydrocarbons were passed through a continuous flow meter, collected in a gas sampling bag and analysed every 20 min, while the catalyst was recovered and characterized only at the end of the reaction.

2.2.3. Product characterization. Mass balance closure was determined by accurately measuring the weights or volumes of all fractions obtained during the hydropyrolysis process, including gas, oil, and solid residues (such as char in the batch reaction system and coke deposited over the catalyst). After each experiment, the total mass of these fractions was compared to the initial mass of the plastic feedstock or the oil pumped. Each experiment consistently achieved a mass balance closure of at least 97 wt%, indicating minimal losses and ensuring the reliability of the experimental results. The small percentage of mass discrepancy (≤3%) could be attributed to minor experimental uncertainties, such as gas sampling or condensation inefficiencies. Relative errors were calculated using data obtained from a reaction that was repeated twice.

Halogen (Cl and Br) contents in char, used catalysts, and oil were determined using active oxidative decomposition (AOD) paired with ion chromatography (IC), according to the EPA 5050 and 9056A standards, using an AOD system from IKA. Detailed procedures and instrumentation were described in a previous work.[16] The alkaline solutions from bubblers, used to trap the eventually generated HCl and HBr, were analysed *via* IC.

Oil samples were analysed by gas chromatography-mass spectrometry (GC-MS) using an Agilent 7820A GC system connected to a 5977B MSD detector, equipped with an HP5-MS UI column (30 m × 0.25 mm × 0.25 mm). Compound identification was carried out using the NIST 2017 spectral library, achieving an average match factor of 85/100, with major compounds typically exceeding 97/100. After grouping the products into families such as monoaromatic hydrocarbons (M-AR), polyaromatic hydrocarbons (P-AR), aliphatic hydrocarbons (ALIPH), oxygenated compounds (O-Comp), and nitrogenated compounds (N-Comp), internal standards were used to calibrate representative compounds from each category, as described in previous research.[33,34]

Gas composition was analysed using a dual-channel Agilent CP 4900 micro-gas chromatograph, equipped with Molsieve 5 Å and HayeSep A columns, and a thermal conductivity detector (TCD). Calibration of the instrument was carried out using standard gas mixtures including N_2, O_2, H_2, CO, CO_2, CH_4, C_2H_4, C_2H_6, C_3H_6, C_3H_8, C_4H_8, and C_4H_{10}. For all these techniques, absolute errors were assessed through multiple analyses.

In order to regenerate the Ni/AC catalyst, the spent catalyst was first washed with Milli-Q water (200 ml g^{-1}) to remove soluble inorganic species, with the filtrate being analysed by IC as described before. This step was followed by washing with dioxane (200 ml g^{-1}), under stirring for 30 minutes, to promote the removal of organic components retained in the catalyst, with the resulting liquid being analysed by GC-MS. After washing, the catalyst was dried overnight at 60 °C and then treated under an inert nitrogen flow (50 ml min^{-1}) at 420 °C for 30 minutes.

3. Results and discussion

The major goal of this work is to assess the performance of Ni-supported catalysts in the hydropyrolysis and dehalogenation of real WEEE plastics, addressing the challenges posed by their complex composition. This is reflected in the data presented in Table 1, showing that this material contains up to 6 different polymers in significant amounts, as well as inorganic components (ashes), heteroatoms (oxygen and nitrogen) and halogens (both Cl and Br). Further details on the composition and properties of the raw plastic were provided in a previous work.[25]

Ni has been selected as the catalytic active phase due to its well-known hydrotreating properties and relatively low cost.[35] On the other hand, four supports (activated carbon, n-ZSM-5 zeolite, silica and alumina) have been selected as they have a very different nature and chemical and textural properties, as described below, which are expected to significantly affect the catalytic behaviour of the Ni phase under hydropyrolysis conditions.

3.1. Catalyst characterization

The N_2 adsorption–desorption isotherms of the four Ni-based catalysts are presented in Fig. S1.† The distinct behaviours observed in the isotherms are directly reflected in their respective textural properties, as summarized in Table 3. The isotherms and textural properties of the corresponding parent

Table 3 Physico-chemical properties of Ni-based catalysts and supports

Catalyst	S_{BET} [a] ($m^2\ g^{-1}$)	S_{EXT} [a] ($m^2\ g^{-1}$)	S_{MIC} [a] ($m^2\ g^{-1}$)	V_{MIC} [a] ($cm^3\ g^{-1}$)	V_{TOT} [a] ($cm^3\ g^{-1}$)	Ni load[b] (wt%)	Acidity[c] (mmol g^{-1})
AC	1017	44	973	0.38	0.39	—	—
Ni/AC	870	32	838	0.33	0.36	2.56	—
n-ZSM-5	389	110	279	0.12	0.38	—	0.44
Ni/n-ZSM-5	379	89	277	0.12	0.38	2.67	0.44
SiO_2	223	223	—	—	0.96	—	—
Ni/SiO_2	225	225	—	—	0.94	2.54	—
Al_2O_3	130	130	—	—	0.81	—	0.50
Ni/Al_2O_3	121	121	—	—	0.62	2.56	0.48

[a] S_{BET}, S_{mic}, S_{ext}, V_T, V_{mic}: BET, micropore, and mesopore/external surface areas, total and micropore volumes, respectively, determined from N_2 adsorption/desorption isotherms. [b] Determined by ICP-OES. [c] Measured by integration of the area under the NH_3-TPD curves.

supports are also included to assess the effect of Ni incorporation.

Ni/AC is the catalyst exhibiting the largest BET surface area (870 $m^2\ g^{-1}$) with a Type I isotherm (IUPAC classification). It shows a sharp rise in nitrogen adsorption at low relative pressures ($P/P_0 < 0.1$), which is characteristic of microporous materials.[36] Likewise, the extended plateau over a broad range of higher relative pressures indicates that, once the micropores are filled, there is minimal adsorption on larger pores or external surfaces, further emphasizing the dominance of microporosity ($V_{TOT} \approx V_{MIC}$). In the same way, the micropore surface area for this material represents about 96% of the BET surface area. Regarding the parent AC support, the Ni/AC sample exhibits reduced adsorption across the entire range of relative pressures, which is also reflected in a decrease in the textural properties. Thus, the different types of pore volumes and surface areas undergo a noticeable reduction after Ni incorporation. In particular, the decrease in V_{MIC} and S_{MIC} by about 14% suggests that a significant portion of the metal is located inside the activated carbon micropores.

As expected, both the Ni/n-ZSM-5 sample and its parent support exhibit high adsorption at low relative pressures (Type I isotherms) arising from the zeolitic micropores. Moreover, as this material is a nanocrystalline zeolite, its isotherm also shows significant adsorption at intermediate and high relative pressures, which agrees well with its relatively large surface area. Nevertheless, in contrast to the activated carbon support, the incorporation of Ni into the n-ZSM-5 zeolite has minimal effect on the micropore surface/volume, while reducing the external surface area. This finding is a clear indication that the Ni species are located outside the zeolite nanocrystals and not within the micropores.

Both Ni/SiO_2 and Ni/Al_2O_3 exhibit Type IV isotherms, which are characteristic of mesoporous materials.[37,38] This is confirmed by the pore size distributions presented in Fig. S1C,† showing the presence of mesopore peaks centred at about 200–230 Å. The distribution is narrower in the case of Ni/SiO_2, whereas Ni/Al_2O_3 is somewhat extended beyond the meso-macropore limit. Ni/SiO_2 has a higher overall adsorption capacity (0.94 $cm^3\ g^{-1}$), a larger BET surface area (225 $m^2\ g^{-1}$) and a more pronounced hysteresis loop, confirming a well-developed mesoporous structure. On the other hand, Ni/Al_2O_3 exhibits the lowest surface area (121 $m^2\ g^{-1}$). Taking the parent supports as references, the textural properties of the silica support can be observed to be little affected by the Ni incorporation. However, some reduction in the total pore volume and BET surface area is observed in the case of alumina, which can be associated with changes occurring in this material during the thermal treatments (calcination and reduction) after the Ni impregnation step.

SEM images with EDS elemental mapping were taken to further investigate the dispersion of Ni on the different supports. Fig. 2 shows the distribution of nickel across the catalyst supports, as determined by X-ray microanalysis. In the case of alumina and activated carbon, a high dispersion of Ni particles can be observed. In contrast, a less uniform distribution, with some aggregates of nickel particles, is observed over the silica and n-ZSM-5 supports.

The Ni particle size distribution for the different catalysts was determined from TEM analyses (Fig. 2A–D). The mean size of the detected Ni particles increases in the following order: alumina (2.4 nm) < ZSM-5 (4.6 nm) < activated carbon (7.3 nm) < silica (8.8 nm). However, it should be highlighted that, as indicated above, the incorporation of Ni into the activated carbon reduces both the volume and surface of micropores, suggesting that Ni nanoparticles are not only distributed over its external surface, but are also significantly located inside the AC micropores, making them hard to distinguish in TEM images.

XRD patterns of the different catalysts and supports are shown in Fig. S2.† In the case of AC, a prominent peak at 24.1° is observed, which corresponds to the layered arrangement typical of graphitic carbon (002), while the additional weaker peak at 43.5° reflects the presence of less-ordered carbon regions.[39] This combination suggests that this material contains both graphitized (ordered) and amorphous (non-ordered) carbon structures. The broad and weak nature of these peaks indicates that a significant portion of the carbon remains disordered, despite some localized graphitization. For the n-ZSM-5 sample, the diffraction signals align well with those typical of the MFI zeolitic structure.[40] The XRD pattern of Al_2O_3 shows reflections characteristic of gamma-alumina (γ-Al_2O_3).[41] Finally, the SiO_2 sample exhibits a broad signal at 22° corresponding to amorphous silica,[42] in agreement with the disordered structure of this material.

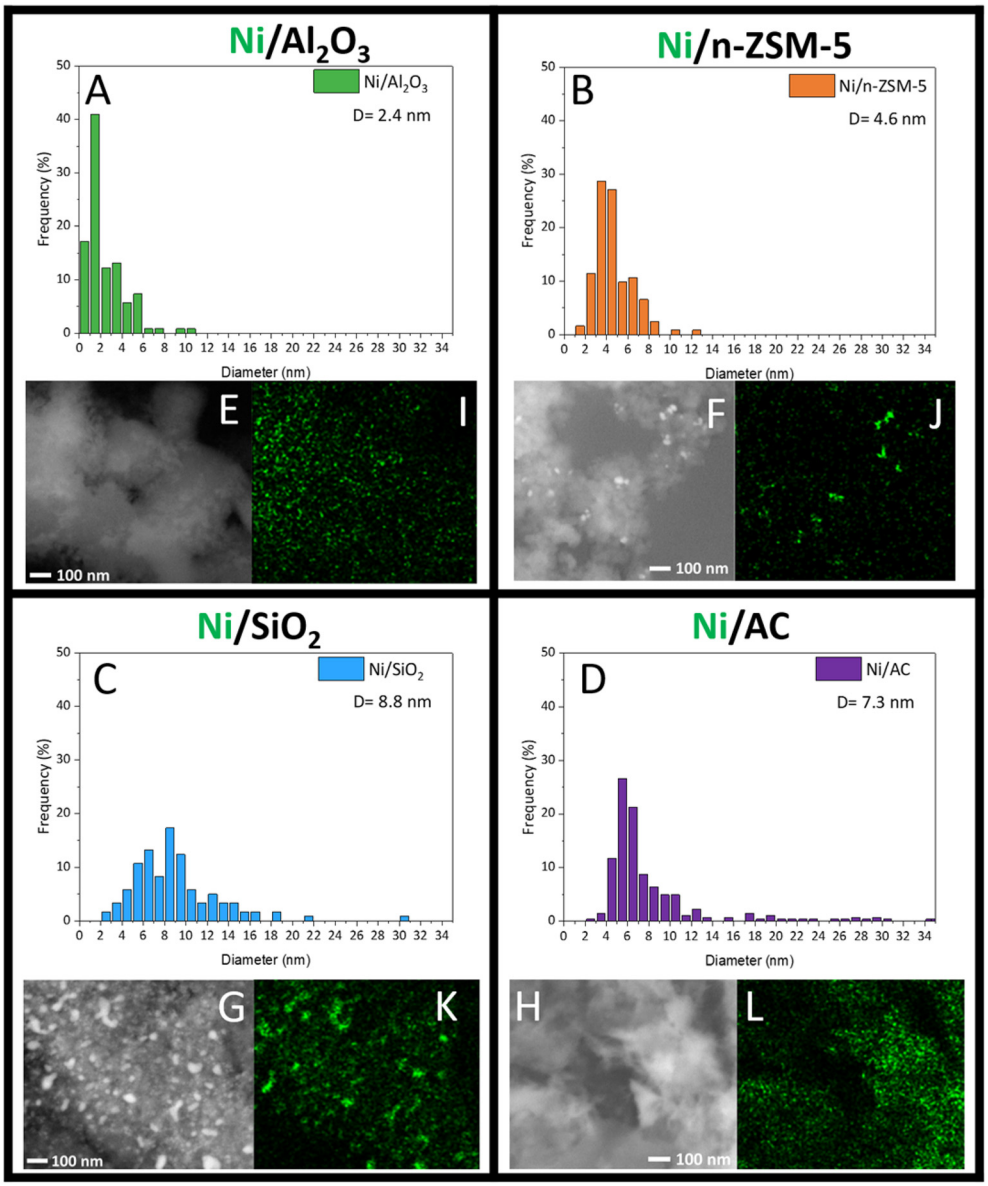

Fig. 2 Size distribution of Ni nanoparticles in the catalysts calculated from TEM images (A–D). SEM images of the catalyst: backscattered electron images (E–H) and nickel mapping (I–L).

After Ni incorporation into the SiO_2 support, a peak at 44° is observed, which can be assigned to the (111) plane of Ni, but with very low intensity. No peaks arising from crystalline metallic Ni can be clearly detected in the rest of the samples, which are typically found at 2θ values around 44°, 51°, and 76° corresponding to the (111), (200), and (220) planes, respectively. The absence of these peaks suggests that the Ni particles are highly dispersed in all the supports and present in very small sizes. It should be highlighted that the Ni content, determined by ICP-OES and shown in Table 3, matches well with the theoretical value for all the materials (2.5 wt%), indicating that the nickel loading during the synthesis process is highly precise and effective. In the case of alumina, during calcination, the generation of a $NiAl_2O_4$ spinel phase on γ-Al_2O_3 is possible in the form of a thin layer that is not detectable by XRD, as previously reported.[43]

The TPD-NH_3 profiles for Ni/Al_2O_3 and Ni/n-ZSM-5 are displayed in Fig. S3,† providing insights into the acidity of these catalysts, based on the desorption of ammonia (NH_3), which interacts with acidic sites on the catalyst surface. NH_3-TPD of Ni/Al_2O_3 indicates substantial acidity (480 μmol g^{-1}, Table 3) with ammonia desorption ranging from 125 to 500 °C, suggesting the presence of a wide variety of acid strengths. Regarding Ni/n-ZSM-5, two different peaks are observed that contribute to a total acidity of 440 μmol g^{-1} (Table 3). In both cases, as shown in Table 3, the acidity remains almost constant after Ni impregnation. Finally, the other two materials, Ni/AC and Ni/SiO_2, exhibit practically no acidity, confirming

the lack of acid sites on the silica and activated carbon supports.

3.2. Screening of catalysts in the hydropyrolysis of WEEE plastics (batch reaction system)

The results obtained from the hydropyrolysis experiments with the WEEE plastic feedstock using the batch reaction system are described below. This section aims to identify the best catalysts in terms of oil halogen removal and upgrading of the liquid product. The product distribution according to fractions (char, oil, gas and coke) is shown in Fig. 3A. The char, accumulated in the thermal zone of the reaction system, is the second largest product, accounting for around 20 wt%. As expected, its yield remains practically constant regardless of the catalyst used. The oil is the major fraction obtained in all the reactions, especially in the thermal one (*ca.* 74 wt%). It slightly decreases in the presence of catalysts due to the enhanced production of gases and the formation of carbonaceous deposits (coke) on the catalysts. Nevertheless, the gas yields never exceed 10 wt%. This stream contains valuable components such as light olefins and paraffins (C2–C4), produced by cracking reactions, and methane, as can be observed in Fig. 3B. The Ni/SiO_2 sample produces the highest CH_4 yield (4.5 wt%) among the tested catalysts while also inhibiting CO_2 production, with a similar but less pronounced effect observed for the Ni/Al_2O_3 catalyst. These results suggest that CO_2 methanation could be playing a significant role in this system, converting CO_2 into CH_4 by hydrogenation and thereby reducing CO_2 emissions. Furthermore, other reactions, such as the cracking/hydrogenation of specific functional groups, present in the different polymers contained in the feedstock, may also contribute to CH_4 formation and influence the product distribution. Additionally, Ni/Al_2O_3 exhibits the lowest production of olefins and paraffins, while the yields of these components are nearly identical for the other three catalysts (≈2.3 and 2.5 wt%, respectively). On the other hand, coke yield ranges between 1.5 and 4 wt%, with Ni/Al_2O_3 showing the lowest value.

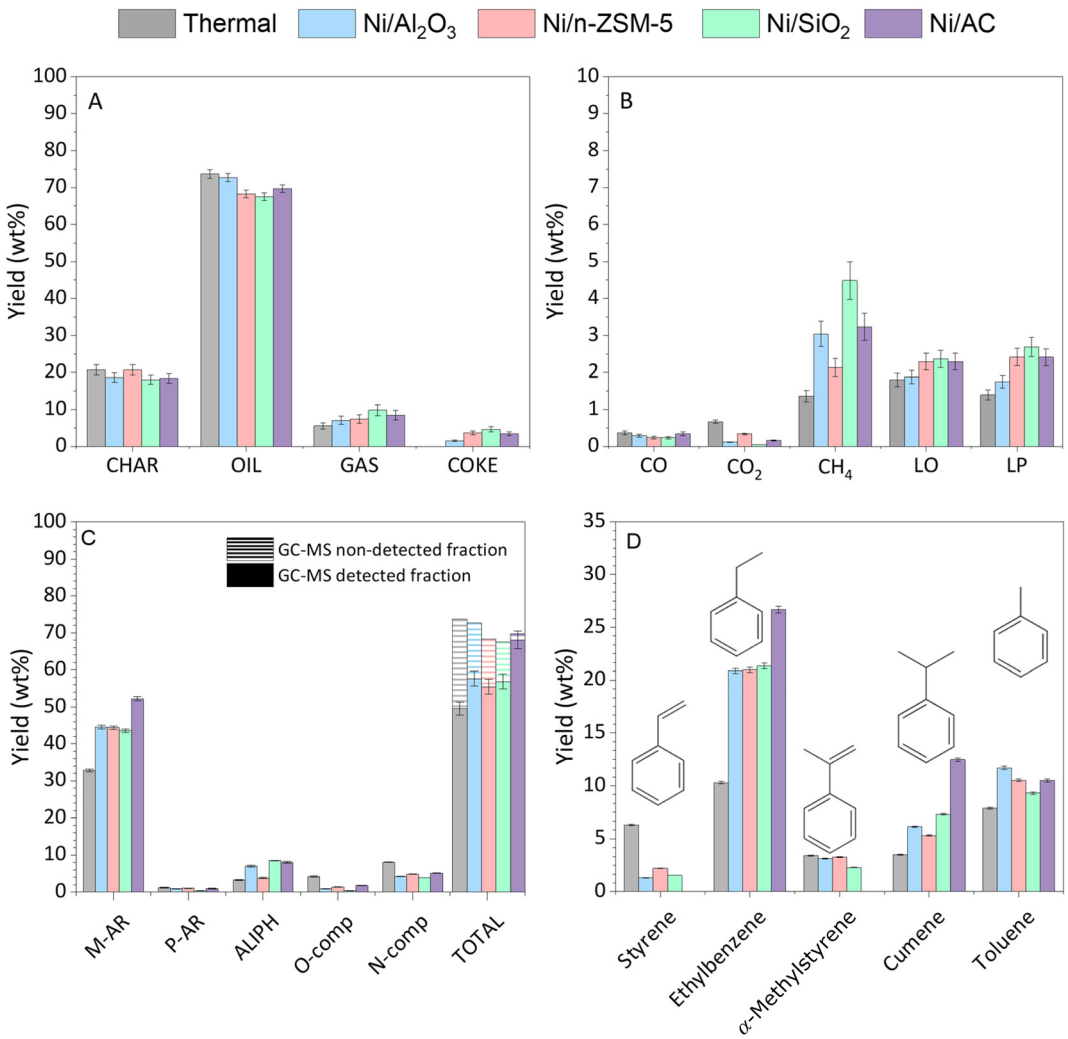

Fig. 3 Hydropyrolysis of WEEE plastics (6 bar, 550/350 °C): (A) fraction yields and (B) gaseous component yields; GC-MS analyses of oils produced: (C) yields of components by families and (D) yields of major compounds in the monoaromatic hydrocarbon family.

The yield of the oil fraction detected by GC-MS, as well as the distribution of components by families, is shown in Fig. 3C. In the thermal reaction, the total yield of components detected by GC-MS is approximately 50 wt% relative to the initial feedstock. The "GC-MS non-detected fraction" mainly consists of heavy compounds, probably oligomers, which have either not been fully cracked or have been formed through secondary radical recombination reactions between primary pyrolysis vapours. These compounds are not detected by GC-MS due to their high molecular weight. In addition, this fraction includes minor compounds that have not been included among those quantified due to their small relative area. The mass yield of this fraction has been quantified by the difference between the total oil yield and the total yield of components detected by GC-MS. A detailed list of the quantified species in the oil fraction is provided in the ESI in Table S1.† All catalysts increase the yield of the detected fraction in comparison with the thermal test. Interestingly, this mainly affects the production of monoaromatic hydrocarbons, which are valuable components with applications as raw chemicals or in the formulation of fuels. The Ni/Al_2O_3, Ni/SiO_2 and Ni/n-ZSM-5 catalysts enhance the oil quality, achieving yields of the GC-MS detected fraction between 55 wt% and 58 wt%. However, the best results are obtained with the Ni/AC sample, which leads to a yield of the detectable fraction of 67 wt%. This figure accounts for 98 wt% of the total oil obtained, being enriched in monoaromatics (52 wt%).

Fig. 3D shows the major compounds within the monoaromatic family (ethylbenzene, cumene and toluene). A hydrogenation effect on the double bonds of the side chains, promoted by all catalysts, becomes evident. This is demonstrated by the decrease in styrene yield in favour of ethylbenzene and of α-methylstyrene production in favour of cumene, when comparing the catalytic tests with the thermal reaction. This effect is particularly pronounced in the case of activated carbon, where styrenic compounds disappear entirely, leading to a corresponding increase in ethylbenzene and cumene. Hydrogenation of double bonds may also have an important effect on the yield of the GC-MS detected fraction since it may prevent the occurrence of secondary oligomerization reactions.

In addition to the effects on monoaromatics, the catalysts also induce a slight reduction in oxygenated (primarily phenolics) and nitrogenated compounds. This is particularly notable for benzenebutanenitrile, generated from the decomposition of ABS, which is converted into simpler nitriles (such as acetonitrile, propanenitrile, isobutyronitrile, and others) and monoaromatics by the effect of the catalysts.

The catalytic performance observed in the reactions can be closely linked to the chemical and textural properties of the supports, as well as the dispersion of nickel. Activated carbon, with its microporous structure, provides a large internal surface area, promoting the adsorption of components and their subsequent transformation. This is also favoured by the strong affinity of the activated carbon support and the organic components present in the pyrolysis vapours. Moreover, the localization of nickel within the micropores with high dispersion is also expected to promote the extension of hydrotreatment reactions. This combination of factors, which are not present when using the other supports, explains the excellent performance in catalytic hydropyrolysis observed for the Ni/AC system. In contrast, the mesoporous nature of silica and alumina supports implies weaker adsorption and interaction with the organic species. On the other hand, although the n-ZSM-5 zeolite is a microporous material having strong acidity, the characterization results indicate that Ni was mainly deposited outside the micropores. This means that both metal and acid sites are mostly separated and do not work in a cooperative manner, which limits their efficiency for oil upgrading under hydropyrolysis conditions.

A further significant aspect of this study is the comprehensive analysis of the dehalogenation results since the raw WEEE plastics contain significant amounts of both Cl and Br that may strongly hinder the further use of the oil fraction. The solid char, which is produced in the thermal zone of the reaction system, is a very effective halogen trap that retains the majority of the Cl and Br present in the raw WEEE plastics (about 95%). The nature of the char fraction has been studied in our previous works,[16,25,44] showing that its halogen capture capacity can be attributed to its dual-matrix composition: ash and a carbonaceous matrix. The ash contains various inorganic species, including TiO_2, CaO, and MgO, which can interact with halogenated compounds, whereas the carbonaceous matrix also promotes halogen trapping. Nevertheless, the oil produced in the thermal reaction zone still contains significant amounts of both Cl and Br (56 and 106 ppm, respectively), thus hindering its further use or co-processing in refinery units. Accordingly, it is expected that the incorporation of catalysts into the hydropyrolysis system may enhance the oil dehalogenation.

Fig. 4A illustrates the distribution of halogens among the hydropyrolysis products (excluding the char). While only a small proportion of the halogens is detected in the gas fraction (<10%), the incorporation of catalysts notably reduced the share of halogens in the oil fraction compared to the thermal test. This oil dehalogenation is accompanied by an increase in the proportion of halogens detected in the coke deposited over the catalysts. This finding can be explained through two different phenomena: hydrodehalogenation reactions and adsorption of halogenated species. Both processes may proceed in combination since the halides formed by HDH may react or can be adsorbed over the coke deposits, which would be favoured by performing the hydropyrolysis tests under 6 bar pressure.

To further evaluate the oil dehalogenation performance of the different catalysts, Fig. 4B illustrates the concentration of both Cl and Br observed in the liquid products, affording a clearer distinction among the effectiveness of the various supported catalysts. All of them exhibit high efficiency in Br removal, with Br being in most cases below the detection limits. However, decreasing the Cl concentration in the oil proved to be more challenging. This fact can be explained by considering the differences in bond dissociation energies of

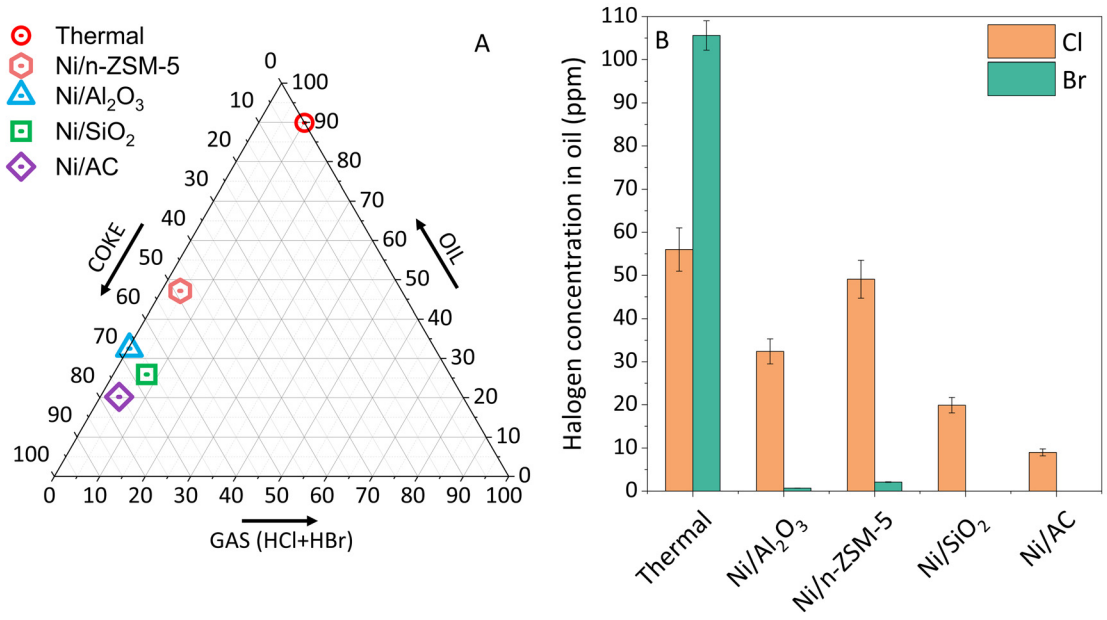

Fig. 4 Hydropyrolysis of WEEE plastics (6 bar, 550/350 °C) with different Ni-based catalysts: (A) triangular diagram of halogenated compound distribution (oil, gas and coke) and (B) Cl and Br concentrations in oil.

C–Br (280 kJ mol^{-1}) and C–Cl (339 kJ mol^{-1}), which agrees well with the greater extent of debromination observed in comparison with the lower levels of dechlorination.[45] Optimal results are obtained with nickel supported on silica and activated carbon. These catalysts achieved complete bromine elimination and reduced chlorine to minimal levels of 20 ppm and 9 ppm, respectively. In contrast, the Ni/n-ZSM-5 catalyst exhibits the poorest dehalogenation performance despite having the highest Brønsted acid site strength and concentration. This inefficiency is likely due to its small micropores (~0.55 nm), which restricts the Ni dispersion and introduces diffusional and steric limitations for bulky components.

The results shown in Fig. 4 indicate that Ni/AC is the best catalyst in terms of oil dehalogenation, as it occurred along with the formation of monoaromatic hydrocarbons. Again, the large surface area, mostly in micropores, of the AC supports and the high Ni dispersion are expected to favour the adsorption and subsequent reaction of both hydrogen and halogenated species over this catalyst during the hydropyrolysis process. In this way, the numerous surface functional groups (such as carboxyl and hydroxyl groups), present in the AC surface, can effectively adsorb halogenated species and break down Cl- and Br-containing compounds.[46]

To assess the possible effects of the activated carbon support, a reaction test was carried out with the AC sample free of Ni (Fig. 5), and the results so obtained were compared with those of Ni/AC and the thermal reference. A significant reduction in the deposition of carbonaceous matter on the catalyst was observed in the presence of nickel compared with the AC reaction test, which was accompanied by enhanced production of the oil fraction. Moreover, a slight increase in the gas yield occurred when incorporating Ni into the catalyst, particularly of methane, due to the higher extension of cracking and hydrogenation reactions. Regarding the oil product distribution, the Ni-containing catalyst leads to a higher production of monoaromatic hydrocarbons compared to the AC support, while also significantly increasing the share and yield of components detected by GC-MS. Likewise, oxygen- and nitrogen-containing species are produced to a lower extent with the Ni/AC catalyst than when using just the support due to the hydrogenation activity of this metal. Concerning the halogen content of the oil, the AC material shows a remarkable removal capacity of both Cl and Br, indicating that this material is able to trap a significant portion of the released halogenated species. However, a notable further improvement in the dehalogenation degree is achieved when adding Ni to the support. Thus, complete bromine elimination only occurs with the Ni/AC catalyst, along with a very small chlorine content (9 ppm). Although these results indicate that there is a significant contribution of the AC support in the dehalogenation process, as it can retain some components, Ni incorporation is needed to achieve a better oil quality and a high degree of dehalogenation.

3.3. Comparison of catalysts in the hydrotreatment of WEEE plastic pyrolysis oil (continuous reaction system)

In this section, Ni/AC and Ni/SiO_2 were selected among the four studied catalysts. Ni/AC was chosen for its overall best performance, while Ni/SiO_2 was included as a reference due to its high dehalogenation efficiency. These catalysts were then tested in a continuous process using an oil generated by the thermal pyrolysis of WEEE plastics, as described in section

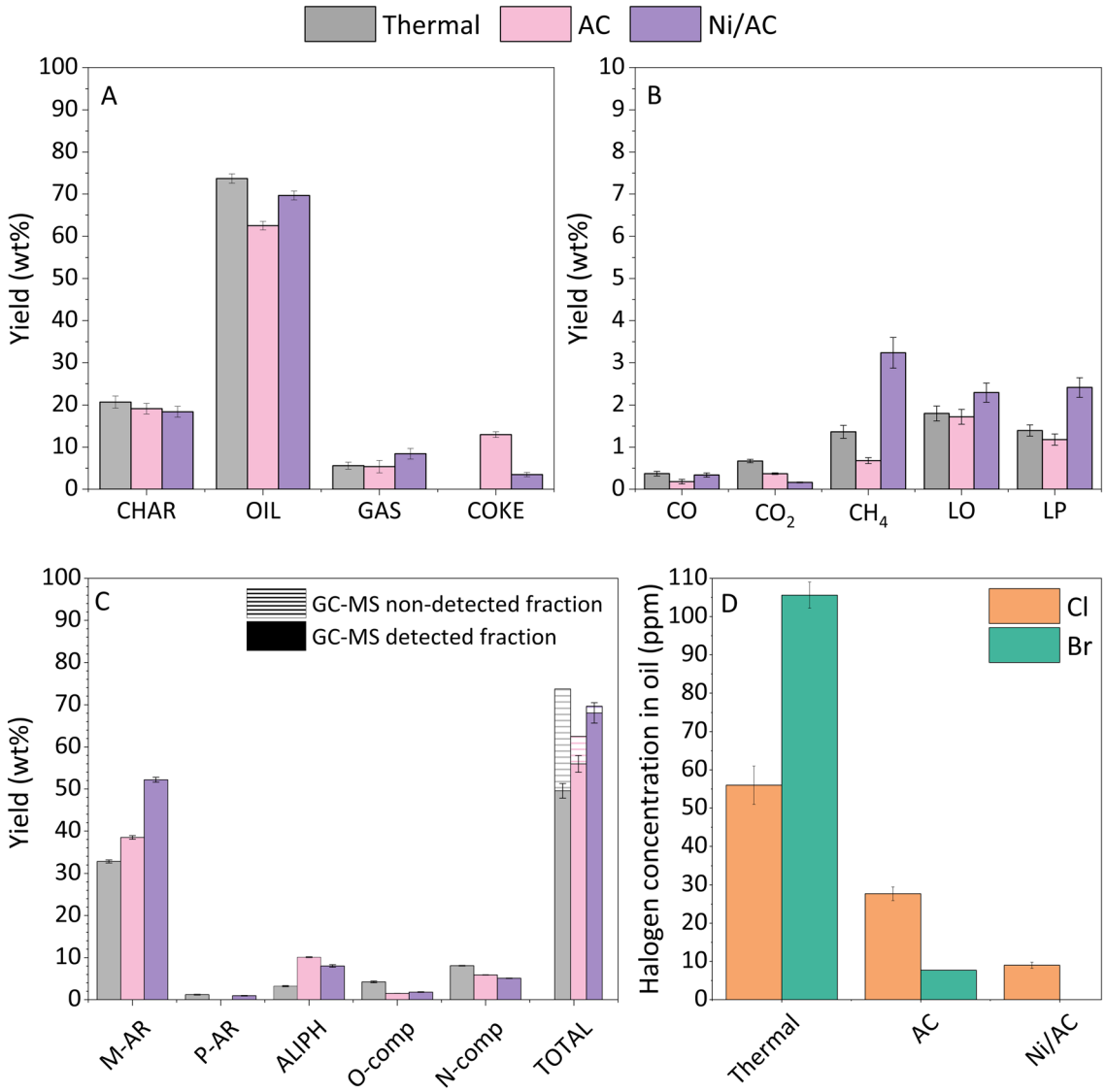

Fig. 5 Effect of the support and Ni incorporation in the hydropyrolysis of WEEE plastics (6 bar, 550/350 °C): (A) fraction yields, (B) gaseous component yields, (C) oil composition detected by GC-MS analysis and (D) halogen content in the oil fraction.

2.2.2. The composition of this oil is given in Table 2 (Feed-1), which shows that it is rich in aromatic hydrocarbons and contains significant concentrations of both Cl and Br. The global mass yields with both catalysts are shown in Fig. 6A.

The hydrotreatment of the pyrolysis oil proceeds with very high liquid yields, in particular when using the Ni/AC catalyst. There is a small production of gases, which can be attributed to the mild temperature used (350 °C), as it prevents cracking reactions to a great extent. Moreover, there is an additional reduction in the oil yield because of the deposition of carbonaceous matter over the catalysts, with this effect being more pronounced for the Ni/SiO_2 sample.

In terms of oil molecular composition (Fig. 6B), the Ni/SiO_2 catalyst reduces the content of monoaromatic compounds in comparison with the raw pyrolysis oil, which in turn also decreases the GC-MS detected fraction. These negative effects may be attributed to the preferential adsorption of these compounds onto the catalyst surface, in agreement with the observed enhanced deposition of carbonaceous matter over this material. Conversely, the Ni/AC catalyst significantly enhances the content of monoaromatic compounds, increasing from 43.4 to 48.1 wt% (relative to the mass of the raw pyrolysis oil) after the hydrotreatment process. This improvement also positively affects the GC-MS detected fraction. The changes observed in the other compound families are comparatively minor.

To gain further insights into these results, the hourly composition of the oil obtained using these two catalysts is summarized in Fig. 7. Overall, the yield of monoaromatics in the case of Ni/SiO_2 decreases over time, consistently remaining lower than their content in the raw oil. Regarding Ni/AC, the yield of monoaromatics also exhibits a decreasing trend over time on stream, although in all cases, it remains higher than

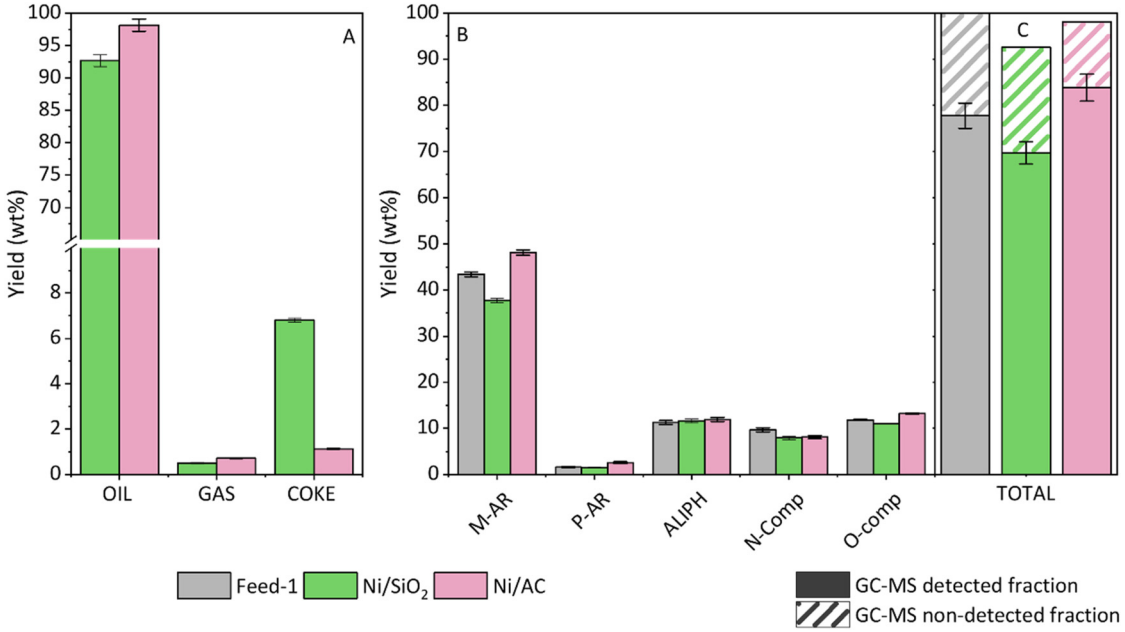

Fig. 6 Cumulative results obtained in the hydrotreatment (350 °C and 6 bar) of the WEEE plastic pyrolysis oil (Feed-1) over Ni/SiO_2 and Ni/AC catalysts using a continuous reaction system: (A) fraction yields; (B) yield of oil components by families; and (C) yield of GC-MS detected and non-detected oil fractions. Grey bars correspond to the raw pyrolysis oil Feed-1.

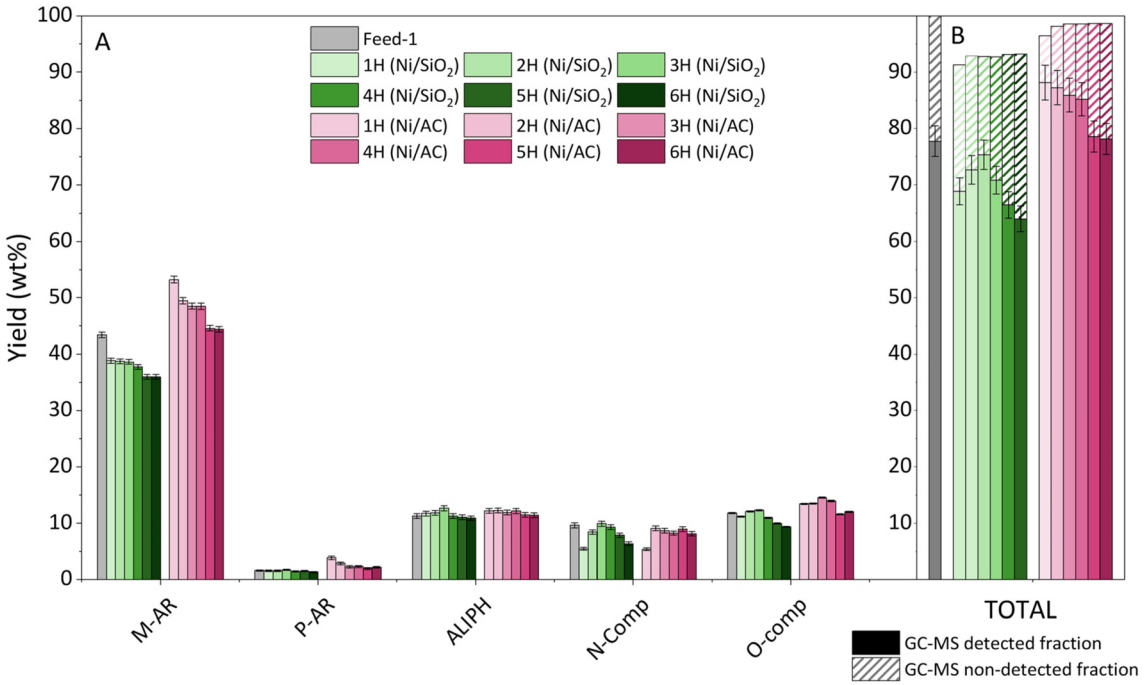

Fig. 7 Hourly results obtained in the hydrotreatment (350 °C and 6 bar) of the WEEE plastic pyrolysis oil (Feed-1) over Ni/SiO_2 and Ni/AC catalysts using a continuous reaction system: (A) yield of oil components grouped by families and (B) yield of GC-MS detected and non-detected oil fractions. Grey bars correspond to the raw pyrolysis oil.

the M-AR content of the raw pyrolysis oil. The feed oil has a low concentration of polyaromatic compounds, and the two catalysts show minimal impact on this fraction, although with some higher P-AR production over the Ni/AC sample. Both catalysts affected N-containing compounds similarly, with a reduction compared to the feed oil during the first hour, followed by an increase to reach values similar to those of the raw pyrolysis oil. On the other hand, the yield of both oxygenated

and aliphatic families shows no significant differences in comparison with the liquid feedstock.

Finally, it can be seen that the GC-MS detected components in the case of the Ni/SiO_2 sample increase considerably during the initial three hours on stream, but then start decreasing. For the Ni/SiO_2 catalyst, the yield of GC-MS detected components is reduced over time on stream, with this effect accelerating during the last two hours. These trends indicate that both catalysts suffer some deactivation, although the Ni/AC sample consistently demonstrates superior performance to the Ni/SiO_2 material in terms of production of monoaromatic hydrocarbons.

Another key aspect is how the catalytic hydrotreatment affects the halogen content of the oil. In this regard, Fig. 8 depicts the global content of both chlorine and bromine in the oil during the entire experiment (Fig. 8A) and the overall degree of oil dehalogenation thus achieved (Fig. 8B). Additionally, the hourly content of chlorine and bromine in the liquid fraction for the two catalysts is shown in Fig. 8C and D, respectively.

Both catalysts effectively reduce the chlorine content, which remains relatively low (below 70 ppm) throughout the reaction test. In contrast, there is a significant difference in the overall bromine removal between the two catalysts (116 ppm with Ni/SiO_2 and 28 ppm with Ni/AC). The dehalogenation degree, shown in Fig. 8B, confirms this trend, with values of 71% and 89% for Ni/SiO_2 and Ni/AC, respectively, relative to the halogen concentration of the liquid feed. Minimal variations in chlorine levels can be observed over time on stream, with Ni/AC slightly outperforming Ni/SiO_2 to maintain lower chlorine concentrations, indicating a slightly better dechlorination activity of the former. Conversely, in the case of bromine, Ni/SiO_2 shows a sharp increase in its concentration, peaking around 180 ppm after 3–4 hours. Meanwhile, Ni/AC maintains much lower bromine levels in the oil, staying consistently below 50 ppm throughout the entire experiment. This indicates that Ni/AC performs better in debromination than Ni/SiO_2 as it is able to maintain its Br removal activity for longer periods of time. Overall, these results highlight Ni/AC as the more effective catalyst for halogen removal, ensuring a cleaner oil product with lower halogen levels.

Fig. 9 compares the dehalogenation efficiency of the catalysts showing the best performance (Ni/AC) for the batch and continuous reaction systems employed here, using the halogen

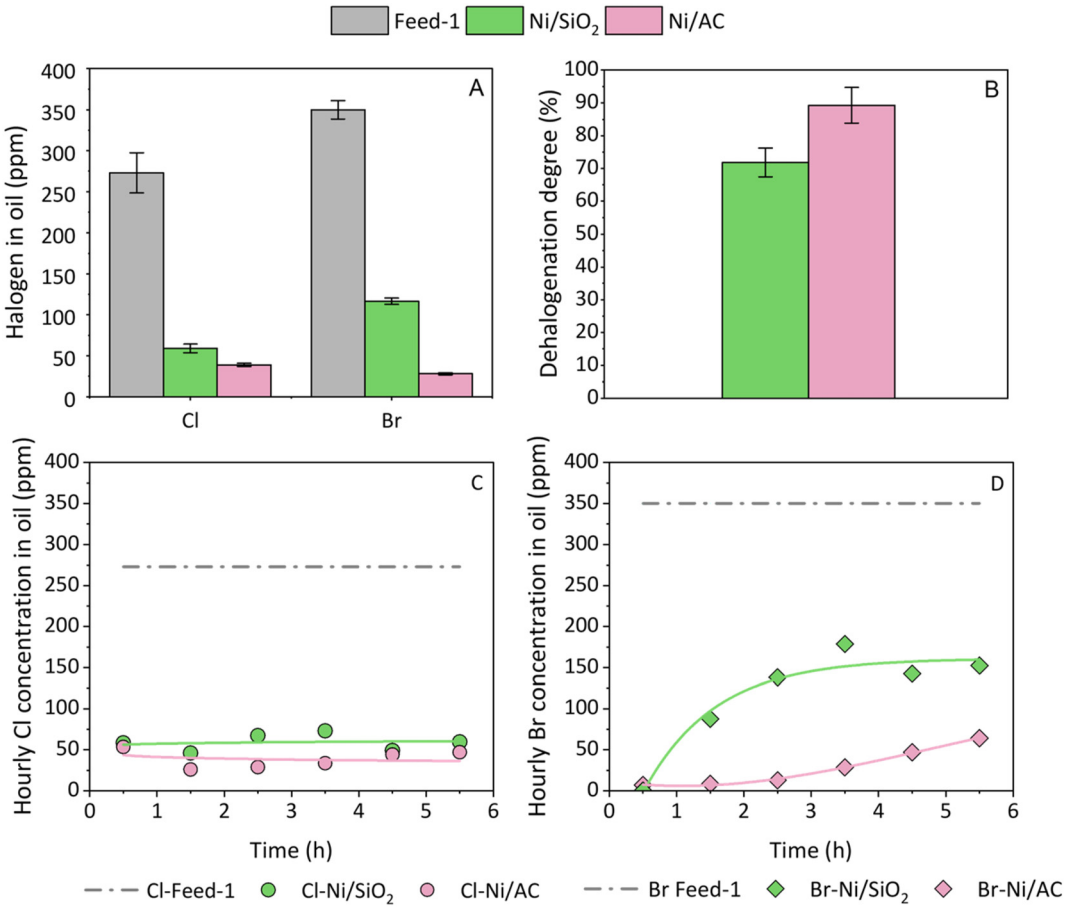

Fig. 8 Overall oil dehalogenation results obtained in the hydrotreatment (350 °C and 6 bar) of the WEEE plastic pyrolysis oil (Feed-1) over Ni/SiO_2 and Ni/AC catalysts using a continuous reaction system: (A) global Cl and Br concentration in the oil; (B) global oil dehalogenation degree; (C) hourly Cl concentration in the oil; and (D) hourly Br concentration in the oil.

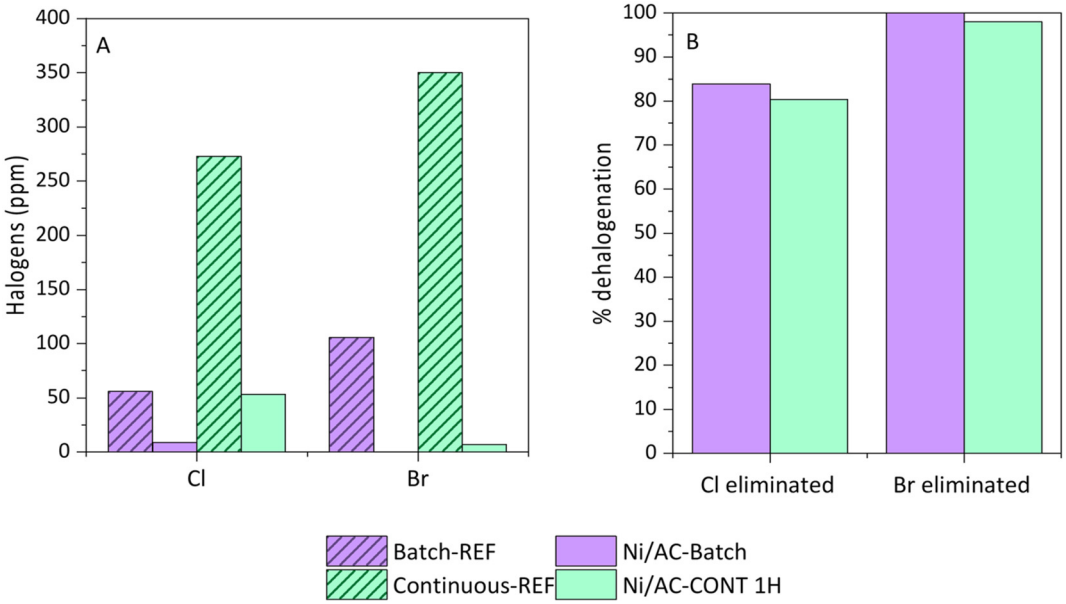

Fig. 9 Comparison of Ni/AC catalyst performance in batch and continuous reactors based on the halogen content (Cl and Br) in the oil fraction. Results include (A) batch and continuous halogen concentrations after 1 h (CONT 1H) and their respective reference values (Batch-REF and Continuous-REF) and (B) the overall dehalogenation degree.

content of the respective thermal oils (Batch-REF and Continuous-REF) as references.

Regarding the Cl content, the batch process shows a significant reduction compared to the thermal test reference, with the level dropping from 56 to 9 ppm (84 wt% dechlorination degree). The continuous reactor provides a higher Cl concentration of the oil (53 ppm after 1 h). However, it should be taken into account that the thermal test reference for the continuous-feeding system (270 ppm) has a higher Cl content; hence, the dechlorination degree (80.4 wt% after 1 h of time on stream) is very similar to that of the batch system. On the other hand, bromine removal in the batch process is very effective, reducing Br content to nearly zero from a reference value of 105 ppm. In the continuous reactor, Br content in the oil after 1 h is also very low (7 ppm) in comparison with the reference thermal test (350 ppm), corresponding to a debromination degree of 98 wt%. These relatively small variations in the dehalogenation performance between both reaction systems can be attributed to the difference in the concentration of components in the gas/vapour phase (higher in the batch system as the feedstock is loaded into the reactor at once and pyrolyzed in just a few minutes). Both reactor configurations offer considerable scale-up potential, each with its own set of advantages. The choice between the two systems will generally depend on factors such as scalability, process efficiency, energy efficiency, product yield, and investment costs.

3.4. Regeneration test

As the catalyst exhibiting the best performance in the hydropyrolysis tests, the Ni/AC sample was selected for regenerability evaluation using a second feedstock (Feed-2), with its properties detailed in Table 2. To that end, the first reaction was carried out with the fresh catalyst and then the spent material was regenerated and reused under the same reaction conditions. Regeneration was performed by solvent (water/dioxane) washing instead of applying an air combustion treatment to avoid damaging the activated carbon support. As shown in Fig. S4,† the fresh and regenerated catalysts behave similarly in terms of yields of the different components detected in the oil fraction. In both cases, small variations were observed in the oil product distribution over time on stream, indicating the high stability of this catalytic system when using this oil as feedstock. Moreover, no significant differences were detected between the fresh and regenerated catalysts in terms of the main oil component family (monoaromatic hydrocarbons).

Regarding the dehalogenation degree, a comparison between fresh and regenerated catalysts is shown in Fig. 10. Chlorine removal is similar for both the fresh and regenerated catalysts (Fig. 10C), maintaining levels below 35 ppm. However, in the case of bromine, the regenerated catalyst appears to perform somewhat better than the fresh one, remaining more stable and keeping bromine levels below 13 ppm after 6 h of time on stream (Fig. 10D). A potential explanation for this unexpected improvement is that the regeneration process may alter the physicochemical properties of the activated carbon support. Specifically, the regeneration could enhance porosity or modify surface functional groups, leading to an increased number of accessible catalytic sites. Thus, the removal of accumulated impurities, coke deposits, or passivating species during regeneration may help restore or even improve the dehalogenation efficiency compared to the fresh sample. However, further studies are required to confirm these hypotheses and fully understand the underlying mechanisms.

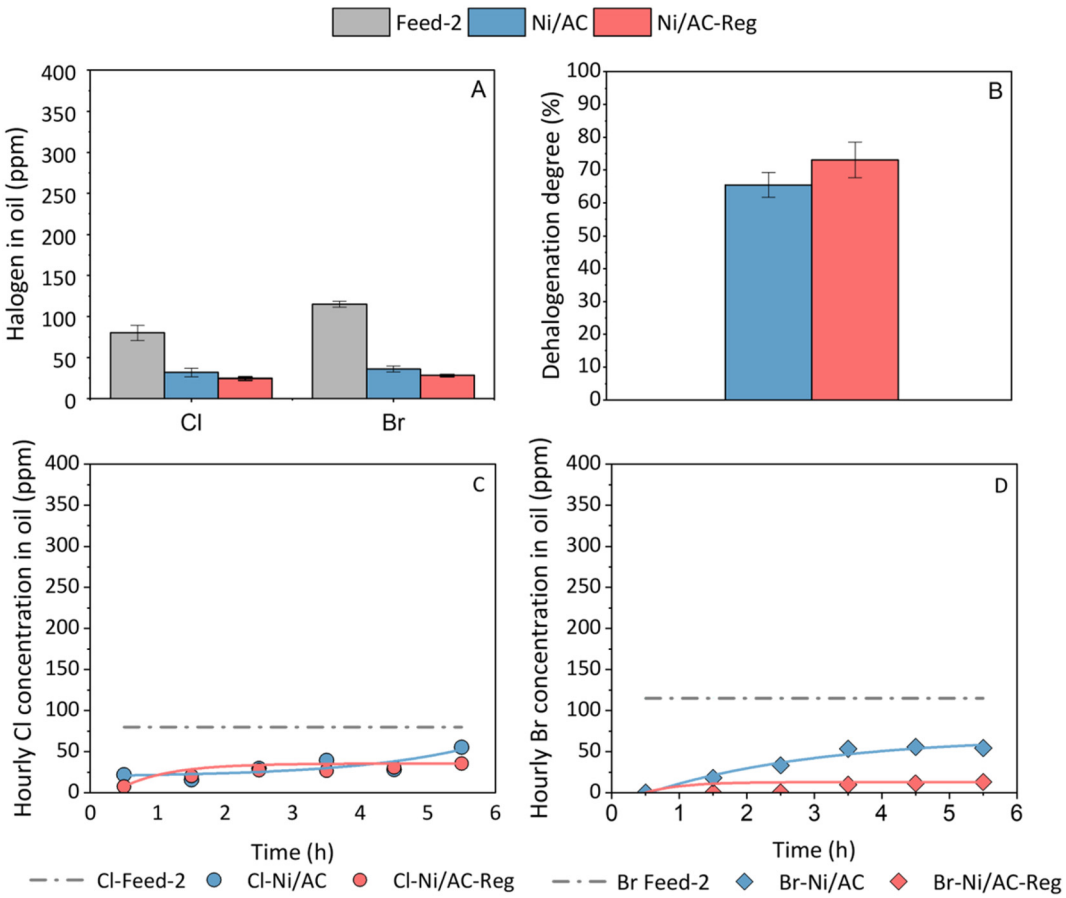

Fig. 10 Oil dehalogenation results obtained in the hydrotreatment (350 °C and 6 bar) of the WEEE plastic pyrolysis oil (Feed-2) over Ni/AC fresh and regenerated catalysts using the continuous reaction system: (A) overall Cl and Br concentrations in the oil; (B) overall oil dehalogenation degree; (C) hourly Cl concentration in the oil; and (D) hourly Br concentration in the oil.

In order to assess the changes in catalyst properties after the reaction and regeneration steps, the spent and regenerated catalysts were characterized using various techniques. From TEM images, it was concluded that the average size of the so detected Ni nanoparticles was practically the same in the fresh and the regenerated catalysts (Fig. S5†), maintaining a high dispersion of the metal species.

TG analyses under an argon atmosphere were performed to gain insights into the accumulation of carbonaceous matter in the AC support (Fig. S6†). The spent catalyst undergoes a much larger weight loss than the fresh one, with two main losses at 315 and 420 °C, which can be related to the adsorption of heavy compounds and the deposition of carbonaceous matter during the reaction test. Moreover, the DTG profile of the fresh catalyst exhibits distinct peaks (200–250 and 475 °C), which disappear after regeneration. This suggests that these peaks could be associated with the elimination of some functional groups, supporting our previous hypotheses, which could explain the observed slight improvement in catalyst debromination after regeneration. Additionally, the solvents used in the regeneration process (water and dioxane) were analysed to evaluate the components extracted. IC analysis of the aqueous solution obtained after catalyst washing revealed that up to 85% of the halogens trapped in the catalyst can be removed with this treatment. Likewise, the solution from the dioxane washing was analysed by GC-MS, showing the presence of both mono- and polyaromatic compounds, such as toluene, benzene and naphthalene, among others, as main components (Table S2†).

Catalyst deactivation in this system could originate from a combination of organic matter deposition and halogen poisoning of the metal sites. Since the catalytic activity can be fully restored by solvent washing of the spent Ni/AC catalyst, it can be envisaged that the major cause of catalyst deactivation, in this case, is the deposition of carbonaceous species, which block the active sites, rather than the poisoning of the metal centres by the formation of Ni halides.

4. Conclusions

Results from this work demonstrate the high potential of catalytic hydropyrolysis for the chemical recycling of waste electrical and electronic equipment (WEEE) plastics.

Using firstly a batch reaction system, nickel supported on Al_2O_3, n-ZSM-5 zeolite, SiO_2 and activated carbon has shown to be highly effective at removing halogens in the oil fraction, with just a slight reduction in the oil yield compared to the non-catalytic test. Likewise, the char generated during the process, and accumulated in the thermal reaction zone, acts as an effective halogen trap. Among the catalysts, Ni/AC exhibits the best oil dehalogenation performance, achieving complete bromine elimination and reducing chlorine content to just 9 ppm. The catalysts also significantly increase the fraction of compounds detectable by GC-MS, enhancing the yield of valuable monoaromatic compounds. These effects are also more pronounced for the Ni/AC catalyst, which is attributed to its high surface area, mainly associated with micropores in which Ni is incorporated with high dispersion.

During the operation of a continuous reaction system, for the hydrotreatment of a WEEE plastic pyrolysis oil with high halogen content, both Ni/SiO_2 and Ni/AC maintain liquid yields exceeding 90 wt% and effectively reduce the halogen content in the oil, although Ni/SiO_2 experiences faster deactivation over time.

For the Ni/AC system, the support is not completely inert in the process, as it can retain some components. Hence, Ni incorporation is needed to achieve better oil quality and a high degree of dehalogenation. Moreover, the Ni/AC catalyst can be regenerated by water/dioxane washing, which facilitates the removal of most of the halogens and carbonaceous matter trapped and accumulated during the hydropyrolysis process, fully restoring its catalytic activity.

Data availability

The data underlying this study are available in the published article.

Conflicts of interest

There are no conflicts to declare.

Acknowledgements

The authors gratefully acknowledge the financial support from the European Union Horizon 2020 program under Grant Agreement No. 820895 (NONTOX Project) and from MICIU/AEI (10.13039/501100011033) and ERDF/EU under Grant Agreement No. PID2023-147355OB-C21 (HYPY-CAT).

References

1 S. Iman, S. Rahman, M. Z. Rahman, B. Saha and Z. Salsabil, in *Comprehensive Materials Processing*, Elsevier, 2024, pp. 125–152.
2 A. Dhandapani, S. Krishnasamy, S. M. K. Thiagamani, D. Periasamy, C. Muthukumar, T. K. Sundaresan, S. Ali and R. Kurniawan, *Recycling*, 2024, **9**, 8.
3 Plastics Europe, *Plastics - the fast facts 2023*, 2023.
4 H. Li, H. A. Aguirre-Villegas, R. D. Allen, X. Bai, C. H. Benson, G. T. Beckham, S. L. Bradshaw, J. L. Brown, R. C. Brown, V. S. Cecon, J. B. Curley, G. W. Curtzwiler, S. Dong, S. Gaddameedi, J. E. García, I. Hermans, M. S. Kim, J. Ma, L. O. Mark, M. Mavrikakis, O. O. Olafasakin, T. A. Osswald, K. G. Papanikolaou, H. Radhakrishnan, M. A. Sanchez Castillo, K. L. Sánchez-Rivera, K. N. Tumu, R. C. Van Lehn, K. L. Vorst, M. M. Wright, J. Wu, V. M. Zavala, P. Zhou and G. W. Huber, *Green Chem.*, 2022, **24**, 8899–9002.
5 R. Kiener, Plast. Pollut., **https://ourworldindata.org/plastic-pollution**.
6 H. Luo, H. Tyrrell, J. Bai, R. Ibrahim Muazu and X. Long, *Green Chem.*, 2024, **26**, 11444–11467.
7 M. S. Qureshi, A. Oasmaa, H. Pihkola, I. Deviatkin, A. Tenhunen, J. Mannila, H. Minkkinen, M. Pohjakallio and J. Laine-Ylijoki, *J. Anal. Appl. Pyrolysis*, 2020, **152**, 104804.
8 Y. V. Vazquez and S. E. Barbosa, *Waste Manag.*, 2016, **53**, 196–203.
9 B. Beccagutti, L. Cafiero, M. Pietrantonio, S. Pucciarmati, R. Tuffi and S. Vecchio Ciprioti, *Sustainability*, 2016, **8**, 1107.
10 A. Soler, J. A. Conesa and N. Ortuño, *Energies*, 2018, **11**, 2612.
11 R. Tiwari, N. Azad, D. Dutta, B. R. Yadav and S. Kumar, *Sci. Total Environ.*, 2023, **881**, 163433.
12 A. J. Martín, C. Mondelli, S. D. Jaydev and J. Pérez-Ramírez, *Chem*, 2021, **7**, 1487–1533.
13 X. Jiang, B. Zhu and M. Zhu, *Green Chem.*, 2023, **25**, 6971–7025.
14 J. Wang, J. Jiang, X. Dong, Y. Zhang, X. Yuan, X. Meng, G. Zhan, L. Wang, Y. Wang and A. J. Ragauskas, *Green Chem.*, 2022, **24**, 8562–8571.
15 K. N. Yogalakshmi, T. Poornima Devi, P. Sivashanmugam, S. Kavitha, R. Yukesh Kannah, S. Varjani, S. AdishKumar, G. Kumar and J. Rajesh Banu, *Chemosphere*, 2022, **286**, 131824.
16 J. Cueto, G. Pérez-Martin, L. Amodio, M. Paniagua, G. Morales, J. A. Melero and D. P. Serrano, *Chemosphere*, 2023, **339**, 139784.
17 K. Ragaert, L. Delva and K. Van Geem, *Waste Manag.*, 2017, **69**, 24–58.
18 J. Gutzeit, *NACE - Int. Corros. Conf. Ser*.
19 M. Kusenberg, A. Eschenbacher, M. R. Djokic, A. Zayoud, K. Ragaert, S. De Meester and K. M. Van Geem, *Waste Manag.*, 2022, **138**, 83–115.
20 M. A. Keane, *ChemCatChem*, 2011, **3**, 800–821.
21 X. Yang, L. Sun, J. Xiang, S. Hu and S. Su, *Waste Manag.*, 2013, **33**, 462–473.
22 F. L. P. Resende, *Catal. Today*, 2016, **269**, 148–155.
23 W. Chen, J. Lu, C. Zhang, Y. Xie, Y. Wang, J. Wang and R. Zhang, *J. Anal. Appl. Pyrolysis*, 2020, **147**, 104800.
24 T. L. Marker, L. G. Felix, M. B. Linck and M. J. Roberts, *Environ. Prog. Sustainable Energy*, 2012, **31**, 191–199.

25 L. Amodio, J. López, A. Souza, J. Cueto, H. Hernando, P. Pizarro and D. Serrano, *J. Hazard. Mater.*, 2024, **465**, 133357.
26 M. A. Keane, *Appl. Catal., A*, 2004, **271**, 109–118.
27 A. Arevalo-Bastante, M. A. Álvarez-Montero, J. Bedia, L. M. Gómez-Sainero and J. J. Rodriguez, *Appl. Catal., B*, 2015, **179**, 551–557.
28 F. D. Kopinke, K. Mackenzie and R. Köhler, *Appl. Catal., B*, 2003, **44**, 15–24.
29 R. F. Howe, *Appl. Catal., A*, 2004, **271**, 3–11.
30 M. R. Flid, L. M. Kartashov and Y. A. Treger, *Catalysts*, 2020, **10**, 216.
31 D. Kim, H. Kang, H. Park, S. Park, J. C. Park and K. H. Park, *Eur. J. Inorg. Chem.*, 2016, **2016**, 3469–3473.
32 J. López, L. Amodio, M. Alonso-Doncel, J. Cueto, H. Hernando, M. Mazur, J. Čejka, P. Pizarro and D. P. Serrano, *J. Environ. Chem. Eng.*, 2024, **12**, 111790.
33 M. Pagano, H. Hernando, J. Cueto, I. Moreno and D. P. Serrano, *Catal. Today*, 2023, **418**, 114065.
34 A. Lago, H. Hernando, J. M. Moreno, D. P. Serrano and J. Fermoso, *Fuel Process. Technol.*, 2021, **215**, 106746.
35 A. R. Ardiyanti, S. A. Khromova, R. H. Venderbosch, V. A. Yakovlev, I. V. Melián-Cabrera and H. J. Heeres, *Appl. Catal., A*, 2012, **449**, 121–130.
36 A. El Nemr, R. M. Aboughaly, A. El Sikaily, M. S. Masoud, M. S. Ramadan and S. Ragab, *Carbon Lett.*, 2022, **32**, 229–249.
37 M. M. Ibrahim, H. S. El-Sheshtawy, M. O. Abd El-Magied and A. S. Dhmees, *Int. J. Environ. Anal. Chem.*, 2023, **103**, 2948–2964.
38 V. Krishnan, M. Suresh and T. Kalaivani, *IOP Conf. Ser.: Mater. Sci. Eng.*, 2022, **1219**, 012038.
39 J. K. Bediako, E. Kudoahor, C. R. Lim, N. S. Affrifah, S. Kim, M. H. Song and E. Repo, *Waste Manag.*, 2024, **177**, 135–145.
40 R. Li, S. Chong, N. Altaf, Y. Gao, B. Louis and Q. Wang, *Front. Chem.*, 2019, **7**, 505.
41 J. Shi, Y. Chen, T. Liu and H. Liang, *J. Dispersion Sci. Technol.*, 2020, **41**, 1471–1479.
42 D. Wang, H. Wang, H. Cao, S. Tu and J. Xue, *Appl. Phys. A: Mater. Sci. Process.*, 2020, **126**, 423.
43 M. Lo Jacono, M. Schiavello and A. Cimino, *J. Phys. Chem.*, 1963, **2522**, 1044–1050.
44 A. López, I. De Marco, B. M. Caballero, M. F. Laresgoiti and A. Adrados, *Fuel Process. Technol.*, 2011, **92**, 253–260.
45 X. Ma, S. Liu, Y. Liu, G. Gu and C. Xia, *Sci. Rep.*, 2016, **6**, 25068.
46 D. Santoro, V. De Jong and R. Louw, *Chemosphere*, 2003, **50**, 1255–1260.